OPTIMAL PROGRAMS TO REDUCE THE RESISTANCE OF GROUNDING SYSTEMS

Run Xiong[1, *], Bin Chen[1], Cheng Gao[1], Yan-Xin Li[1], and Wen Yang[2]

[1]National Key Laboratory on Electromagnetic Environment and Electro-Optical Engineering, PLA University of Science and Technology, Nanjing, Jiangsu 210007, China

[2]Engineering and Design Institute, Chengdu Military Area of PLA, Kunming 650222, Yunnan, China

Abstract—In this paper, some optimal programs have been proposed through the analyses of transient grounding resistance (TGR) to reduce the grounding resistance using the finite-difference time-domain method. First, the TGR of various electrode types, lengths and sectional programs is studied, and it is found that a flat bar is the most financially efficient conductor to be used as grounding electrode. Enlarging grounding electrode length can reduce grounding resistance when it is shorter than the effective length, but the reduction effect declines as the length increases. Additionally, a series of small electrodes would lead to a much lower resistance than a single large one. Second, it is demonstrated that locally improving the soil near the grounding system is an efficient way of reducing the grounding resistance. Improving a limited area soil surrounding the lifting line would reduce the peak resistance significantly, while local enlarging electrodes surrounded soil conductivity can reduce the grounding system steady resistance obviously.

1. INTRODUCTION

Grounding systems with various configurations of grounding electrodes is often a part of lightning protection systems [1–11]. Grounding system provides a channel that current passes by, and large current flows through the grounding system before dissipating in the ground when lightning strikes. The surpassed voltage and radiation by the

current are mainly determined by the resistance of the grounding system. Therefore, it is necessary to find the optimized programs to reduce the grounding system resistance.

The finite-difference time-domain (FDTD) method [12–25], which provides a simple and efficient way of solving Maxwell's equations for a variety of problems, has been widely applied to solve many types of electromagnetic problems. The FDTD method has been used to investigate the transient characteristics of grounding systems since 2001 [26].

When uniform grid FDTD method is used to analyze grounding systems, huge computational resources will be involved because of the electrically small size of the grounding electrode compared with the whole computational domain. In this paper, non-uniform FDTD grids are used to simulate the area near the lifting line and the electrode in order to model the electrode with fine grids without resulting in huge computational resources.

The grounding system performance is analyzed in the form of transient grounding resistance (TGR), which reflects the dynamic behavior of a grounding system. The TGR reaches it peak grounding resistance value at the beginning time of the transient current's dissipating to the ground, and then tends to the steady state as the current vary speed decreases.

The TGR of the three commonly used conductors is analyzed to find the most financially efficient configuration to be used as the grounding electrode. The TGR of various electrode lengths is also analyzed to find the optimized approaches. Additionally, the TGR of a group of small electrodes is compared with that of a single large electrode of the same sectional size to get the optimal program.

With the development of the compound materials, the problem caused by the traditional resistance-reducing-agent has been overcome. The new water-absorbent compound material can reduce the resistance dramatically, and work for a long time without corrosion against the grounding electrode [27]. In Section 4, the resistance-reducing-agent is used to enlarge the conductivity and the relative permittivity of the local soil near the grounding system. The effect of the parameter and dimension of the locally improved soil near the lifting line and the vertical electrode is analyzed respectively, and some useful conclusions are drawn to reduce the grounding system resistance.

2. THE CALCULATION MODEL

To calculate the TGR, the computational model in [2–6] is adopted, as shown in Fig. 1(a). Only homogenous ground is considered in this,
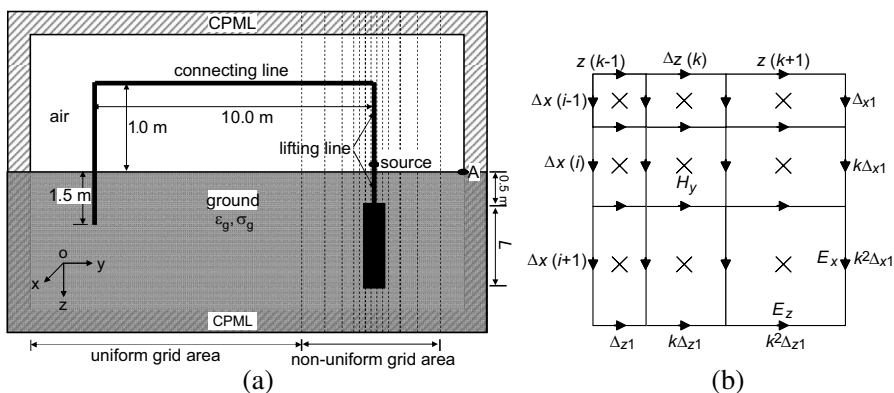
Figure 1. The TGR calculation model. (a) The whole computational domain. (b) The nearby grids in the non-uniform area.

paper and it is assumed that the ground has a steady constitutive parameter. The conductivity is set at $\sigma_g = 0.004\,\mathrm{S/m}$ and the relative permittivity of the ground is $\varepsilon_g = 9.0$.

The lightning current pulse can be modeled by

$$\mathbf{I}(t) = kI_0 \left(e^{-\alpha t} - e^{-\beta t} \right) \tag{1}$$

where $k = 1.1016$, $I_0 = 5.0 \times 10^4\,\mathrm{V/m}$, $\alpha = 3.7618 \times 10^4\,\mathrm{s^{-1}}$, $\beta = 1.13643 \times 10^8\,\mathrm{s^{-1}}$. The mainly power (99.94%) is under the frequency 10MHz.

The TGR is defined as a ratio of the transient voltage to the transient current

$$R_t = V_t / I_t \tag{2}$$

where I_t is the transient current flowing through grounding electrode, which can be defined from the Ampere's Law

$$\begin{aligned} I_t = {} & [H_z(i - 1/2, j + 1/2, k) - H_z(i + 1/2, j + 1/2, k)]\Delta_z \\ & + [H_x(i, j + 1/2, k + 1/2) - H_x(i, j + 1/2, k - 1/2)]\Delta_x \end{aligned} \tag{3}$$

By integrating the electric field along the air-ground interface from the computational domain boundary (point E of Fig. 1(a)) to the lifting line, the transient voltage V_t can be obtained

$$V_t = \sum_{j=N_l}^{N_a} V_j = - \sum_{j=N_l}^{N_a} E_j \Delta s_j \tag{4}$$

where N_l and N_a are FDTD mesh indexes of the point of the lifting line entering ground and the point E of Fig. 1 respectively.

In this paper, efforts have been made to reduce both the peak grounding resistance (referred as peak resistance, which is the peak value of R_t) and the steady grounding resistance (referred as steady resistance, which is the resistance value when R_t do not vary with time obviously, e.g., at $1.5\,\mu$s).

To model the grounding electrode area accurately, the non-uniform standard FDTD method is involved [28]. The grounding electrodes are always several meters long while electrically small in the sectional area dimensions [1]. Therefore, non-uniform grids in two dimensions are occupied while a uniform grid in the length dimension is used. The time-stepping equations for the electric and magnetic fields E_y and H_y read

$$E_y^{n+1}(i,j+1/2,k) = \frac{\varepsilon_y - 0.5\Delta t\sigma_y}{\varepsilon_y + 0.5\Delta t\sigma_y} E_y^n(i,j+1/2,k)$$

$$+\frac{\Delta t}{\varepsilon_y + 0.5\Delta t\sigma_y} \left[\begin{array}{c} \dfrac{H_x^{n+1/2}(i,j+1/2,k+1/2) - H_x^{n+1/2}(i,j+1/2,k-1/2)}{0.125(\Delta z(k-1)+6\Delta z(k)+\Delta z(k+1))} \\ -\dfrac{H_z^{n+1/2}(i+1/2,j+1/2,k) - H_z^{n+1/2}(i-1/2,j+1/2,k)}{0.125(\Delta x(i-1)+6\Delta x(i)+\Delta x(i+1))} \end{array} \right]$$

$$(5)$$

$$H_y^{n+1/2}(i+1/2,j,k+1/2) = \frac{\mu_y - 0.5\Delta t\sigma_{my}}{\mu_y + 0.5\Delta t\sigma_{my}} H_z^{n-1/2}(i+1/2,j,k+1/2)$$

$$+\frac{\Delta t}{\mu_y + 0.5\Delta t\sigma_{my}} \left[\begin{array}{c} \dfrac{E_x^n(i+1/2,j,k+1) - E_x^n(i+1/2,j,k)}{0.125(\Delta z(k-1)+6\Delta z(k)+\Delta z(k+1))} \\ -\dfrac{E_z^n(i+1,j,k+1/2) - E_z^n(i,j,k+1/2)}{0.125(\Delta x(i-1)+6\Delta x(i)+\Delta x(i+1))} \end{array} \right] \qquad (6)$$

Uniform grid is used for the main areas, where the grid size is $\Delta_x \times \Delta_y \times \Delta_z = 10\,\text{cm} \times 10\,\text{cm} \times 10\,\text{cm}$. The expansion factor is set as $k = k_x = k_z = 1.162$, while uniform grid is used in the y direction, as shown in Fig. 1(b). 20 layers non-uniform grids are used, which results in the smallest cell size $\Delta_{\min} = 0.5\,\text{cm}$ for the electrode areas. The time step is $\Delta t = \Delta_{\min}/2c$, where c is the speed of light in the free space.

With this model, the effect of the electrode configurations and locally improved soil on the TGR is analyzed respectively to find optimized grounding electrode programs.

3. OPTIMAL ELECTRODE CONFIGURATION PROGRAMS

This section focuses on steady resistance, and performance of the grounding electrode is observed at various electrode configurations to seek out optimized programs. First, performances of the three commonly used conductor bars are studied to find out the most economically efficient conductor type which can be used as grounding electrode. Second, the grounding electrode length effect on the TGR is analyzed. Third, the TGR of a group of small electrodes and a single large electrode of the same total sectional size are also compared.

3.1. The Optimal Grounding Electrode Type

In the engineering practice, the three commonly used bars (round bar, square bar and flat bar) [29–33] are commonly used as the grounding electrode. In this part, the TGR of the grounding system is tested when two arrangements bars are used as the grounding electrode.

The sectional sizes of the three commonly used conductor bars are shown in Table 1, whose lengths are all $2.5\,\mathrm{m}$. In Arrangement 1, the three bars are of the same surface area ($0.2\,\mathrm{m}^2$) while the sectional sizes are different. In Arrangement 2, the three bars are of the close cross-sectional area as listed in the ISO standards. The TGR when the two arrangements conductor bars are used as the grounding electrode is shown in Fig. 2.

It can be seen that the TGR of the grounding system varies when different type conductors are used as the electrode. As plotted in Fig. 2(a), the steady resistance is $69.15\,\Omega$, $70.69\,\Omega$ and $71.43\,\Omega$ when the
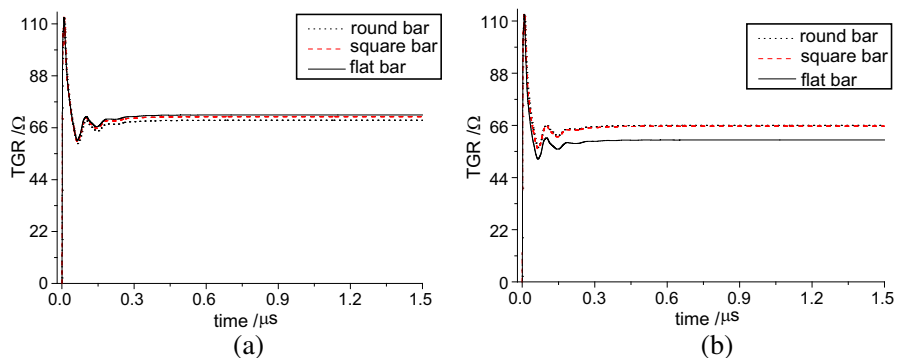

Figure 2. The Time-domain response TGR when different conductor bars are used as the conductor. (a) TGR under Arrangement 1. (b) TGR under Arrangement 2.

Table 1. Configuration of the three conductors.

Arrangement	Types	Round bar	Square bar	Flat bar
	Section			
1	Size (mm)	d=25	d=20	w=35, d=5
	Volume (m^3)	1.23×10^{-3}	1.0×10^{-3}	4.38×10^{-4}
2	Size (mm)	d=35	d=30	w=100, d=5
	Volume (m^3)	2.41×10^{-3}	2.25×10^{-3}	1.25×10^{-3}

round bar, square bar and flat bar are used as the grounding electrode respectively. Though the round bar leads to a lower steady resistance, 3.2% than the flat electrode, the conductor material volume is 2.8 times than the flat bar. The grounding resistance of the square bar is 1.1% smaller than the flat bar, while the conductor material usage is 2.3 times than the flat bar.

Figure 2(b) graphs the TGR when the bars of arrangement 2 are used as the grounding electrode. The resistance of the round bar and the square bar is nearly the same, and steady resistance is about 66.6 Ω for the round bar and square bar while 60.6 Ω for the flat bar. The conductor material volume of the round bar and square bar is about two times of the flat bar in arrangement 2. From comparison of Fig. 2(b) with Fig. 2(a), it can also be seen that large electrode sectional size of the same type bar would result in a lower grounding resistance.

From the analyses above, it can be concluded that large electrode size would result in a lower grounding resistance, and flat bar is the most financially efficient among the three conductor types to be used as the grounding electrode in the engineering practice.

3.2. The Electrode Length Effect on the TGR

According to Type *A* arrangement in IEC 62305-3 [1], the vertical electrode is 2.5 m in length. In this part, the electrode length effect on the TGR is studied. The flat iron, whose sectional size is 30 mm×5 mm, is employed as the grounding electrode, while the length varies from 1.0 m to 50.0 m. The TGR of varied electrode lengths is graphed in Fig. 3.

Figure 3(a) plots the transient time domain response of varied length electrodes, and it can be seen that the electrode length does not affect the peak resistance but longer electrode results in a lower steady resistance. Additionally, the enlarged part of an electrode only affects
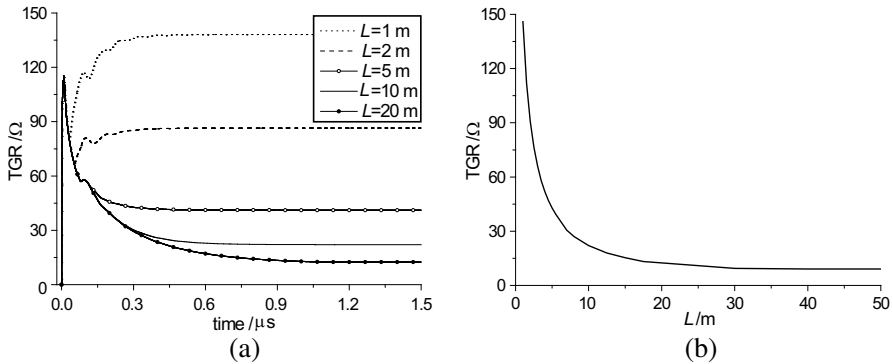
Figure 3. Grounding resistance at different electrode lengths, where L is the electrode length. (a) TGR versus time at varied electrode lengths. (b) Steady resistance versus electrode length L.

the late time TGR rather than the early time TGR, e.g., the TGR of the first $0.4\,\mu s$ is the same under both the conditions $L = 20$ and $L = 10\,m$, but a lower resistance after $0.4\,\mu s$ is gained when $L = 20\,m$.

Figure 3(b) graphs steady resistance at $1.5\,\mu s$ as electrode length L increases from $1\,m$ to $50\,m$. It is clear that the steady resistance decreases as the electrode length increases, but the reduction effect declines as the length increases. When the electrode is longer than $30\,m$, the resistance does not vary obviously, which means the effective length is $30\,m$ for this case. It is worth to note that the effective length obtained here is for the supposed earth resistivity and current, and it is larger for more resistive earth and slow fronted currents pulses [7]. It can also be seen that the grounding resistance decreases rapidly when the electrode is smaller than $10\,m$.

Therefore, it can be concluded that enlarging electrode length can reduce steady resistance when it is shorter than the effective length, but the reduction effect declines as the electrode length increases.

3.3. The TGR of a Single Large Electrode and a Group of Small Electrodes

In this part, the TGR of a group of 5 small electrodes is compared with that of a single large electrode, whose sectional size is the same as the total sectional size of the 5 small electrodes.

The configuration of the 5 small flat bars is shown in Fig. 4(a). The sizes of the 5 small bars are all $2.0\,cm \times 0.5\,cm \times 250.0\,cm$, and the distance from the outer bar to the center bar is all $25.0\,cm$. The TGR of the group of 5 electrodes are graphed in Fig. 4(b), where the
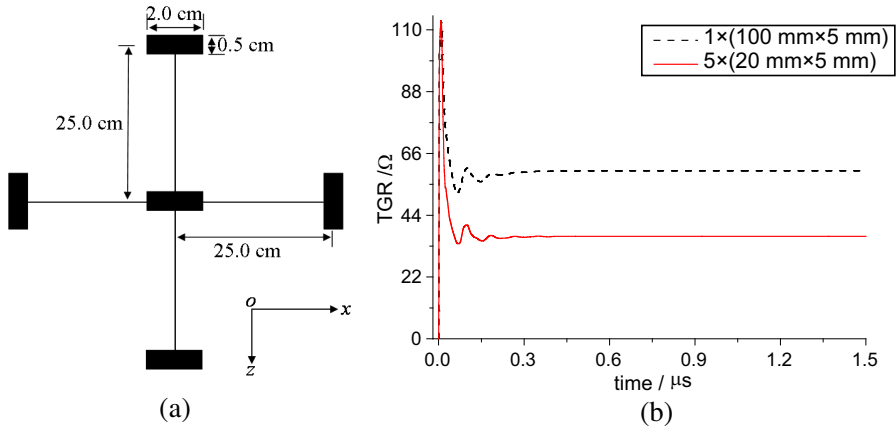
Figure 4. The TGR of a single large bar and a group of small bars. (a) A group of 5 small bars. (b) TGR of a large bar and a group of small bars.

TGR of a single large electrode $(10.0\,\text{cm} \times 0.5\,\text{cm} \times 250.0\,\text{cm})$ is also listed. It can be seen that the grounding resistance is $44.1\,\Omega$ for the series of 5 small flat bars, which is $16.5\,\Omega$ lower than that of the single large flat bar though the volume of the two programs is the same.

Therefore, in the engineering practice, it is more efficient to use a series of small bars instead of a single large bar as the grounding electrodes.

From the analyses in this section, some conclusions can be derived for the engineering practice. First, flat bar is the most financially efficient bar to be used as the grounding electrode among the three commonly used conductors. Second, enlarge the electrode length until the effective length can reduce the resistance, but the reduction effect declines as the length increases. Third, a series of small electrodes would result in a much lower resistance than a single large one.

4. LOCAL LY IMPROVED SOIL EFFECT ON THE TGR

In this section, both the peak resistance and the steady resistance are considered and the soil surrounding the lifting line and the electrode is locally improved by utilizing of resistance-reduce-agent to enlarge the soil conductivity and relative permittivity. The resistance-reduce-agent utilized area is shown in Fig. 5, where the grounding electrode length is 2.5 m. Area I is the locally improved soil surrounding the lifting line whose dimension is $w \times d$. Area II is the locally improved grounding
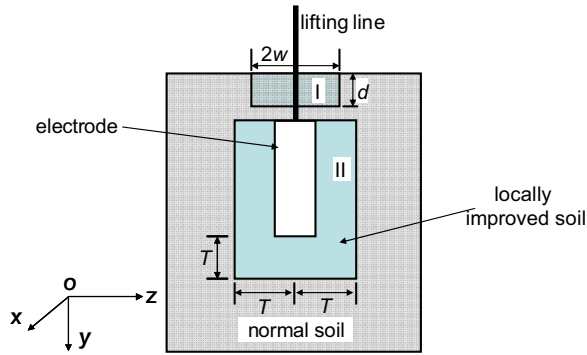
Figure 5. The resistance-reduce-agent utilized area, where area I is the locally improved soil surrounding the lifting line and area II is the locally improved electrode surrounded soil.

electrode surrounded soil, whose dimension is $2T \times 2T \times (T + 2.5\,\text{m})$.

First, only the soil surrounding the lifting line is improved locally, and the locally improved soil dimension and parameter (conductivity and relative permittivity) effect on the TGR is analyzed. Second, only the vertical electrode surrounded soil is improved locally, and effect of the locally improved soil dimension, conductivity and relative permittivity on the TGR is studied.

4.1. Locally Improved Lifting Line Surrounded Soil Effect on the TGR

In this part, the soil surrounding the lifting line is locally improved, while the soil surrounding the grounding electrode is the normal soil. The TGR of various locally improved lifting line surrounded soil dimension and parameters is studied to find the optimized programs.

First, the improved soil width effect on the TGR is analyzed. The depth of the lifting line surrounded soil is set at $d = 0.5\,\text{m}$, and the width is varied from $w = 0.2\,\text{m}$ to $2.0\,\text{m}$. Fig. 6(a) graphs the TGR as the width varies, and it is clear that the steady resistance is reduced steadily as the width of surrounding soil increases. The peak resistance is reduced dramatically from $112.8\,\Omega$ to $99.0\,\Omega$ as the width increase to $w = 0.8\,\text{m}$, but it is not reduced obviously when the locally improved soil width is larger than $w = 1.4\,\text{m}$.

Second, the improved soil depth effect on the TGR is studied. The width of the lifting line surrounded improved soil is $w = 2.0\,\text{m}$, and the depth is varied from $d = 0.1\,\text{m}$ to $0.5\,\text{m}$. Fig. 6(b) graphs the TGR of these cases, and it can be seen that the steady resistance

is reduced steadily as the locally improved soil depth increases. The peak resistance is reduced from $112.8\,\Omega$ to $97.6\,\Omega$ as the depth of the improved soil increases to $d = 0.3\,\text{m}$, but is not reduced obviously as the depth increases.

Third, the conductivity of the locally improved lifting line surrounded soil effect on the TGR is analyzed. The improved soil area surrounding the lifting line is $w \times d = 1.4\,\text{m} \times 0.5\,\text{m}$, and the relative permittivity of the soil is $\varepsilon_{rl} = 9$. The improved soil conductivity is varied from $\sigma_l = 0.01\,\text{S/m}$ to $0.1\,\text{S/m}$, and the TGR is graphed in Fig. 7(a). It can be seen that both the steady resistance and the peak resistance are reduced as the conductivity of the soil surrounding the lifting line increases.

Fourth, the locally improved lifting line surrounded soil relative permittivity effect the on the TGR is studied. The surrounding soil conductivity is $\sigma_l = 0.004\,\text{S/m}$, while the relative permittivity is varied from $\varepsilon_{rl} = 9$ to 80. Fig. 7(b) plots the TGR of these cases, and it can be seen that increase of the relative permittivity can only reduce the TGR value of the first $0.3\,\mu\text{s}$ but has nothing to do with the steady resistance after $0.3\,\mu\text{s}$.

Therefore, the soil surrounding the lifting line should be locally improved to a $1.4\,\text{m} \times 0.3\,\text{m}$ area. Enlarging the relative permittivity of the local soil surrounding the lifting line can reduce the peak resistance dramatically, while locally enlarging the conductivity can both reduce the peak resistance and the steady resistance.
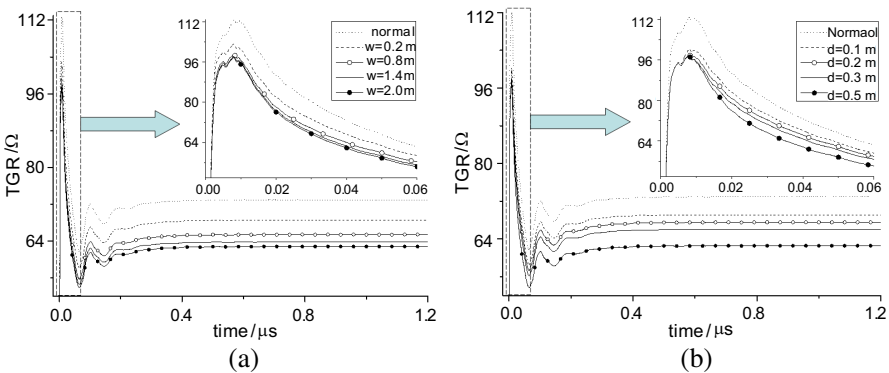

Figure 6. The locally improved lifting line surrounded soil dimension effect on the TGR, where "normal" indicates the case that nothing has been done on the lifting line. (a) TGR of varied improved soil width when $d = 0.5\,\text{m}$. (b) TGR of varied improved soil depth when $w = 2.0\,\text{m}$.
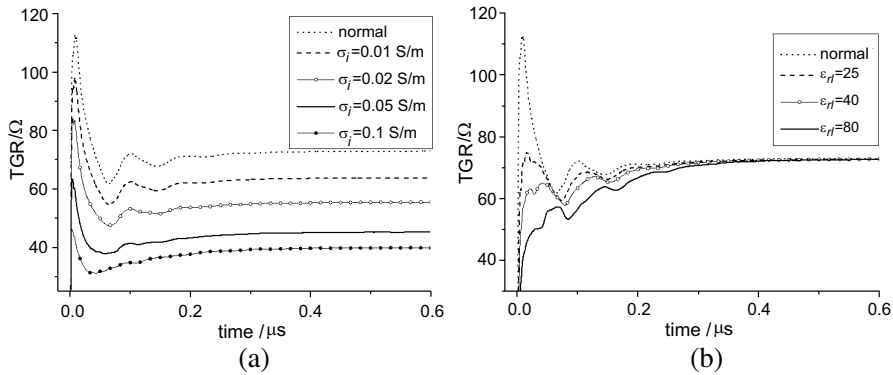
Figure 7. The locally improved lifting line surrounded soil conductivity and relative permittivity effect on the TGR. (a) Conductivity varied when $\varepsilon_{rl} = 9$. (b) Permittivity varied when $\sigma_l = 0.01\,\mathrm{S/m}$.

4.2. Locally Improved Grounding Electrode Surrounded Soil Effect on the TGR

In this part, the soil surrounding the grounding electrode is locally improved, while the soil surrounding the lifting line is the normal soil. The TGR of various locally improved grounding electrode surrounded soil dimension and parameters is studied to find the optimized programs.

First, the conductivity of the soil surrounding the grounding electrode is improved to $\sigma_e = 0.01\,\mathrm{S/m}$ and relative permittivity is $\varepsilon_{re} = 9$, and the TGR is analyzed when the locally improved soil dimension is varied from $T = 0.1\,\mathrm{m}$ to $1.0\,\mathrm{m}$. As can be seen from Fig. 8, the steady resistance is reduced steadily as the improved electrode surrounded soil area increases but the reduction effect declines as the dimension increases continually.

Second, the conductivity effect on the TGR is studied when the locally improved soil conductivity increases from $\sigma_e = 0.01\,\mathrm{S/m}$ to $0.1\,\mathrm{S/m}$. The soil is locally improved at a $2.0\,\mathrm{m} \times 2.0\,\mathrm{m} \times 3.5\,\mathrm{m}$ area, and the relative permittivity is $\varepsilon_{re} = 9$. As can be seen from Fig. 9(a), the steady resistance is reduced steadily as the conductivity of the improved electrode surrounded soil increases. But when the conductivity is larger than $\sigma_e = 0.05\,\mathrm{S/m}$, the steady resistance did not decrease obviously as the local soil conductivity increases.

Third, the relative permittivity of the improved soil surrounding the grounding electrode is varied from $\varepsilon_{re} = 9$ to 80 while $\sigma_e = 0.004\,\mathrm{S/m}$, and the TGR is calculated. As can be seen from Fig. 9(b),
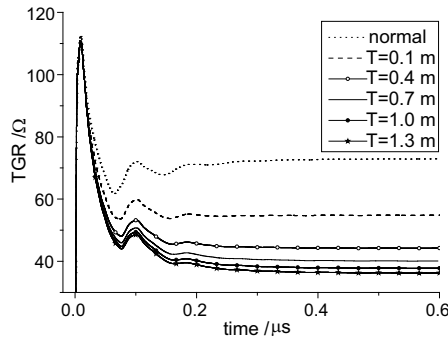
Figure 8. The dimension of the electrode surrounded soil effect on the TGR.
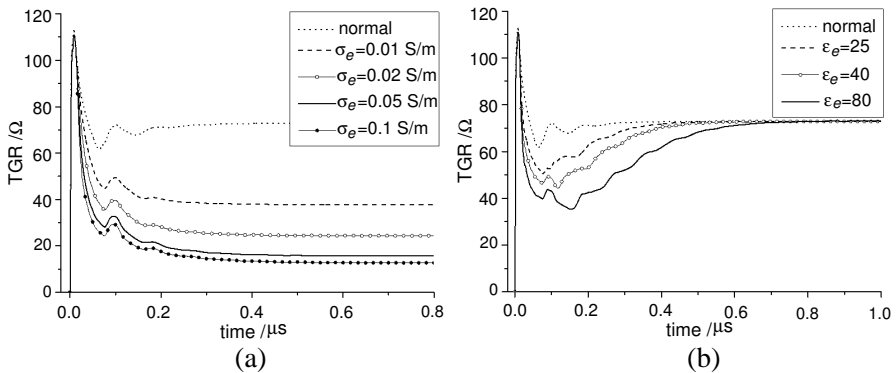

Figure 9. The parameter of the electrode surrounded soil effect on the TGR. (a) TGR of varied conductivity. (b) TGR of varied relative permittivity.

locally enlarging the relative permittivity of the soil surrounding the grounding electrode cannot reduce the peak resistance. However, there would be a significant reduction of the resistance between $0.02\,\mu s$ to $0.5\,\mu s$ as the relative permittivity of the soil surrounding the grounding electrode enlarges. It can also be seen that the relative permittivity of the electrode surrounded soil does not affect the TGR after $0.7\,\mu s$.

Thus, it can be concluded that a large improved soil area surrounding the electrode would result in a lower grounding resistance, but the reduction effect declines as the area increases. Improving the relative permittivity of the soil surrounding the electrode can only reduce the grounding resistance between $0.02\,\mu s$ to $0.5\,\mu s$, while enlarging the electrode surrounded soil conductivity is an effective way of reducing the steady resistance.
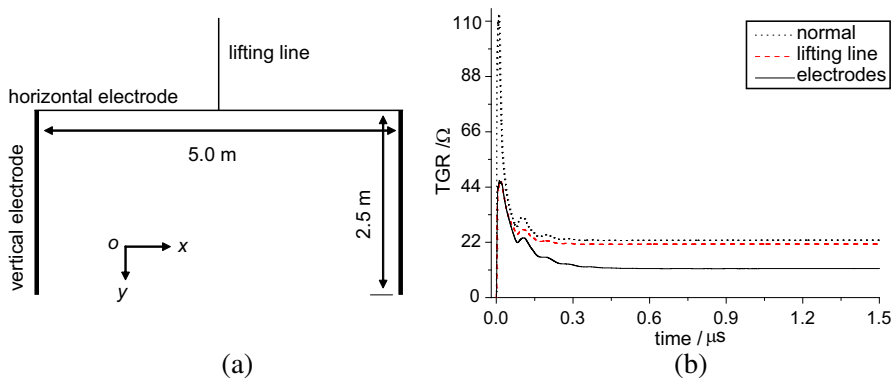
(a)   (b)

Figure 10. The TGR of a grounding system with locally improved soil. (a) The grounding system combined with a horizontal electrode and two vertical electrodes. (b) The grounding system TGR with the proposed approaches, where: - - - indicates the case that the lifting line surrounded soil is improved locally and — indicates the case both the lifting line and the electrodes surrounded soil is improved.

4.3. Locally Improved Soil Effect on the Grounding System TGR

To check the efficiency of the locally improved soil effect on the grounding resistance, the conclusions obtained above are introduced into a grounding system combined with a horizontal electrode and two vertical electrodes as shown in Fig. 10(a) [1].

First, only the lifting line surrounded soil is locally improved in a $1.4\,\mathrm{m} \times 1.4\,\mathrm{m} \times 0.5\,\mathrm{m}$ area, and the soil parameters are improved to $\sigma_l = 0.05\,\mathrm{S/m}$ and $\varepsilon_{rl} = 40$. Second, the two vertical electrode surrounded soil conductivity is improved to $\sigma_e = 0.05\,\mathrm{S/m}$ further in area II as shown in Fig. 5, where $T = 1.0\,\mathrm{m}$. The relative permittivity of the soil surrounding the two electrodes is $\varepsilon_{re} = 9$.

Figure 10(b) graphs the grounding system TGR when the soil is locally improved. It can be seen that the peak resistance is reduced from $112.8\,\Omega$ to $46.4\,\Omega$ when the lifting line surrounded soil parameter is improved, and the steady resistance is also reduced from $22.8\,\Omega$ to $21.3\,\Omega$ in this case. Additionally, the steady resistance is further reduced to $11.5\,\Omega$ as the two grounding electrodes surrounded soil conductivity is enlarged.

From the TGR analyses in this part, we can say that the proposed approaches are efficient ways of reducing both the peak resistance and steady resistance of a grounding system.

From the analysis in this section, it can be concluded that locally improving the soil surrounding the lifting line and grounding electrode is an efficient ways of reducing the grounding resistance. Following conclusions can be obtained:

1. Enlarging the area and conductivity of the improved soil surrounding both the lifting line and the grounding electrode are all efficient ways of reducing the steady resistance.

2. Improving the soil surrounding the lifting line is an efficient way to reduce the peak resistance and the optimal area of the improved lifting line surrounded soil is a $1.4\,\mathrm{m} \times 1.4\,\mathrm{m} \times 0.3\,\mathrm{m}$ area.

3. Locally improving the relative permittivity of the soil surrounding the grounding electrode can only reduce the resistance between $0.02\,\mathrm{\mu s}$ to $0.5\,\mathrm{\mu s}$, but it is unable to reduce the peak or steady resistance.

5. CONCLUSIONS

In this work, the resistance of the grounding system in lightning protection systems has been analyzed using the FDTD method in the form of TGR. First, the electrode configurations effect on the TGR is analyzed to find optimized grounding electrode programs. Second, the resistance-reducing-agent is locally utilized to improve the soil parameters, and the effect of the locally improved soil area and parameters on the TGR is studied. From these analyses, the following conclusions can be derived.

First, flat bar is the most financially efficient structure to be used as the grounding electrode. Enlarging grounding electrode length can reduce grounding resistance when it is shorter than the effective length, but the reduction effect declines as the length increases. Large electrode size would result in a lower grounding resistance, but it would be more efficient to use a series of small electrodes rather than a single large one.

Second, locally improving the soil near the grounding system is an efficient way of reducing the grounding system resistance. Enlarging the area and conductivity of the soil surrounding both the lifting line and grounding electrodes locally are all efficient ways of reducing the steady resistance. Improving the soil surrounding the lifting line is an efficient way to reduce the peak resistance and the optimal area of the improved lifting line surrounded soil is a $1.4\,\mathrm{m} \times 1.4\,\mathrm{m} \times 0.3\,\mathrm{m}$ area.

The conclusions derived in this paper would be useful in the grounding system design.

ACKNOWLEDGMENT

REFERENCES

1. IEC 62305-3. Ed.1, *Protection Against Lightning-Part 3: Physical Damage to Structures and Life Hazard*, 2006.

2. Visacro S. and R. Alipio, "Frequency dependence of soil parameters: Experimental results, predicting formula and influence on the lightning response of grounding electrodes," *IEEE Trans. on Power Delivery*, Vol. 27, No. 2, 927–935, 2012.

3. Zeng R., J. L. He, Y. Q. Gao, J. Zou, and Z. C. Guan, "Grounding resistance measurement analysis of grounding system in vertical-layered soil," *IEEE Trans. on Power Delivery*, Vol. 19, No. 4, 1553–1559, 2004.

4. Meliopoulos A. P. S., S. Patel, and G. J. Cokkinides, "A new method and instrument for touch and step voltage measurement," *IEEE Trans. on Power Delivery*, Vol. 9, No. 4, 1850–1860, Oct. 1994.

5. Tsumura M., Y. Baba, N. Nagaoka, and A. Ametani, "FDTD simulation of a horizontal grounding electrode and modeling of its equivalent circuit," *IEEE Trans. on Electromagnetic Compatibility*, Vol. 48, No. 4, 817–825, 2006.

6. Xiong R., B. Chen, J.-J. Han, Y.-Y. Qiu, W. Yang, and Q. Ning, "Transient resistance analysis of large grounding systems using the FDTD method," *Progress In Electromagnetic Research*, Vol. 132, 159–175, 2012.

7. Grcev, L., "Impulse efficiency of grounding electrodes," *IEEE Trans. on Power Delivery*, Vol. 24, No. 1, 441–451, 2009.

8. Izadi, M., M. Z. A. Ab Kadir, and C. Gomes, "Evaluation of electromagnetic fields associated with inclined lightning channel using second order FDTD-hybrid methods," *Progress In Electromagnetics Research*, Vol. 117, 209–236, 2011.

9. Izadi, M., M. Z. A. Ab Kadir, and C. Gomes, "Evaluation of lightning current and velocity profiles along lightning channel using measured magnetic flux density," *Progress In Electromagnetics Research*, Vol. 130, 473–492, 2012.

10. Izadi, M., M. Z. A. Ab Kadir, C. Gomes, and V. Cooray, "Evaluation of lightning return stroke current using measured

electromagnetic fields," *Progress In Electromagnetics Research*, Vol. 130, 581–600, 2012.

11. Gomes, C. and M. Z. A. A. Kadir, "Protection of naval systems against electromagnetic effects due to lightning," *Progress In Electromagnetics Research*, Vol. 113, 333–349, 2011.

12. Taflove, A. and S. C. Hagness, *Computational Electrodynamics: The Finite-difference Time-domain Method*, 3rd Edition, Artech House, 2005.

13. Lee, K. H., I. Ahmed, R. S. M. Goh, E. H. Khoo, E. P. Li, and T. G. G. Hung, "Implementation of the FDTD method based on Lorentz-Drude dispersive model on GPU for plasmonics applications," *Progress In Electromagnetics Research*, Vol. 116, 441–456, 2011.

14. Kong, Y.-D. and Q.-X. Chu, "Reduction of numerical dispersion of the six-stages split-step unconditional-stable FDTD method with controlling parameters," *Progress In Electromagnetics Research*, Vol. 122, 175–196, 2012.

15. Sirenko, K., "An FFT-accelerated FDTD scheme with exact absorbing conditions for characterizing axially symmetric resonant structures," *Progress In Electromagnetics Research*, Vol. 111, 331–364, 2011.

16. Cao, D.-A. and Q.-X. Chu, "FDTD analysis of chiral discontinuities in waveguides," *Progress In Electromagnetics Research Letters*, Vol. 20, 19–26, 2011.

17. Mao, Y.-F., B. Chen, H.-Q. Liu, J.-L. Xia, and J.-Z. Tang, "A hybrid implicit-explicit spectral FDTD scheme for the oblique incidence programs on periodic structures," *Progress In Electromagnetics Research*, Vol. 128, 153–170, 2012.

18. Ai, X., Y. Han, C. Y. Li, and X.-W. Shi, "Analysis of dispersion relation of piecewise linear recursive convolution FDTD method for space-varying plasma," *Progress In Electromagnetics Research Letters*, Vol. 22, 83–93, 2011.

19. Kong, L.-Y., J. Wang, and W.-Y. Yin, "A novel dielectric conformal FDTD method for computing SAR distribution of the human body in a metallic cabin illuminated by an intentional electromagnetic pulse (IEMP)," *Progress In Electromagnetics Research*, Vol. 126, 355–373, 2012.

20. Kong, Y.-D., Q.-X. Chu, and R.-L. Li, "Study on the stability and numerical error of the four-stages split-step FDTD method including lumped inductors," *Progress In Electromagnetics Research B*, Vol. 44, 117–135, 2012.

21. Xiong R., B. Chen, Y. Mao, B. Li, and Q.-F. Jing, "A simple local approximation FDTD model of short apertures with a finite thickness," *Progress In Electromagnetics Research*, Vol. 131, 135–152, 2012.

22. Vaccari A., A. Cala′ Lesina, L. Cristoforetti, and R. Pontalti, "Parallel implementation of a 3D subgridding FDTD algorithm for large simulations," *Progress In Electromagnetics Research*, Vol. 131, 135–152, 2012.

23. Salski, B., "The unfolding of bandgap diagrams of hexagonal photonic crystals computed with FDTD," *Progress In Electromagnetics Research M*, Vol. 27, 27–39, 2012.

24. Lesina, A. C, A. Vaccari, and A. Bozzoli, "A novel RC-FDTD algorithm for the drude dispersion analysis," *Progress In Electromagnetics Research M*, Vol. 27, 27–39, 2012.

25. Gutierrez, G. G., S. F. Romero, J. Alvarez, S. G. Garcia, and E. P. Gil, "On the use of FDTD for hirf validation and certification," *Progress In Electromagnetics Research Letters*, Vol. 32, 145–156, 2012.

26. Tanabe, K., "Novel method for analyzing dynamic behavior of grounding systems based on the finite-difference time-domain method," *IEEE Power Engineering Review*, Vol. 21, 55–57, 2001.

27. Yamane, H., T. Idegucri, M. Tokuda, and H. Koga, "Long-term stability of reducing ground resistance with water absorbent polymers," *IEEE ISEMC*, 678–682, Tokyo, Japan, 2011.

28. Yu, W.-H. and R. Mittra, "A technique of improving the accuracy of the non-uniform time-domain algorithm," *IEEE Trans. on Microw. Theory Tech.*, Vol. 47, No. 3, 353–356, 1999.

29. ASTM B152/B152M–13: *Standard Specification for Copper Sheet, Strip, Plate, and Rolled Bar*, 2009.

30. ASTM B272–12: *Standard Specification for Copper Flat Products with Finished (Rolled or Drawn) Edges (Flat Wire and Strip)*, 2009.

31. ISO 1035-1, *Hot-rolled Steel Bars-Part 1: Dimensions of Round Bars*, 1980.

32. ISO 1035-2, *Hot-rolled Steel Bars-Part 2: Dimensions of Square Bars*, 1980.

33. ISO 1035-3, *Hot-rolled Steel Bars-Part 3: Dimensions of Flat Bars*, 1980.